frontiers

Conceptual models of entrainment, jet-lag, and seasonality

Isao T. Tokuda [1], **Christoph Schmal** [2], **Bharath Ananthasubramaniam** [3] and **Hanspeter Herzel** [2,3,*]

[1] *Department of Mechanical Engineering, Ritsumeikan University, Kusatsu-shi, Shiga, Japan.*

[2] *Institute for Theoretical Biology, Humboldt Universität zu Berlin, Berlin, Germany.*

[3] *Institute for Theoretical Biology, Charité - Universitätsmedizin Berlin, Berlin, Germany.*

Correspondence*:
Hanspeter Herzel
h.herzel@biologie.hu-berlin.de

2 ABSTRACT

3 Understanding entrainment of circadian rhythms is a central goal of chronobiology. Many
4 factors, such as period, amplitude, *Zeitgeber* strength, and day-length, govern entrainment
5 ranges and the phase of entrainment. Using global optimization, we derive conceptual models
6 with just three free parameters (period, amplitude, relaxation rate) that reproduce known
7 phenotypic features of vertebrate clocks: relatively small phase response curves (PRCs), fast re-
8 entrainment after jet-lag, and seasonal variability to track light onset or offset. Since optimization
9 found multiple sets of model parameters, we can study this model ensemble to gain insight into
10 the underlying design principles. We find that amplitudes control the size of PRCs, that fast
11 relaxation supports short jet-lag, and that specific periods allow reasonable seasonal phase
12 shifts. *Arnold* onions of representative models visualize strong dependencies of entrainment on
13 periods, relative *Zeitgeber* strength, and photoperiod.

14 **Keywords: circadian rhythms, amplitude-phase model, parameter optimization, jet-lag, phase response curve, entrainment,**
15 **seasonality**

1 INTRODUCTION

16 1.1 Entrainment and oscillator theory

17 The circadian clock can be regarded as a system of coupled oscillators, be it the neuronal network in
18 the SCN (Hastings et al., 2018) or the 'orchestra' of body clocks (Dibner et al., 2010). Furthermore, the
19 intrinsic clock is entrained by *Zeitgebers* such as light, temperature and feeding. The concept of interacting
20 oscillators (Huygens, 1986; Van der Pol and Van der Mark, 1927; Kuramoto, 2012; Strogatz, 2004) can
21 contribute to the understanding of entrainment (Winfree, 1980). The theory of periodically driven self-
22 sustained oscillators is based on the concept of "*Arnold* tongues" (Pikovsky et al., 2003; Granada et al.,
23 2009). *Arnold* tongues mark the ranges of periods and *Zeitgeber* strengths in which entrainment occurs
24 (Abraham et al., 2010). The range of periods over which entrainment occurs is called the "range of
25 entrainment" (Aschoff and Pohl, 1978). If seasonal variations are also considered, the entrainment regions
26 have been termed "*Arnold* onions" (Schmal et al., 2015). Within these parameter regions, amplitudes and

27 entrainment phases can vary drastically. Amplitude expansion due to periodic forcing is termed resonance
28 (Duffing, 1918). Of central importance in chronobiology is the variability of the entrainment phase,
29 since the coordination of the intrinsic clock phase with the environment provides evolutionary advantages
30 (Aschoff, 1960; Ouyang et al., 1998; Dodd et al., 2005).

1.2 Phenomenological amplitude-phase models

32 After the discovery of transcriptional feedback loops (Hardin et al., 1990), many mathematical
33 models focussed on gene-regulatory networks (Leloup and Goldbeter, 2003; Forger and Peskin, 2003;
34 Becker-Weimann et al., 2004). However, most available data on phase response curves (PRCs) (Johnson,
35 1992), entrainment ranges (Aschoff and Pohl, 1978), and phases of entrainment (Rémi et al., 2010)
36 are based on organismic data. Thus it seems reasonable, to study phenomenological models that are
37 directly based on these empirical features. There is a long tradition of heuristic amplitude-phase models
38 in chronobiology (Klotter, 1960; Wever, 1962; Pavlidis, 1973; Daan and Berde, 1978; Winfree, 1980;
39 Kronauer et al., 1982).

40 Here, we examine the limits of the capability of such heuristic amplitude-phase models to reproduce
41 fundamental properties of circadian entrainment. To this end, we combine the traditional amplitude-phase
42 modeling approach with recent oscillator theory and global optimization to identify minimal models that
43 can reproduce essential features of mammalian clocks: relatively small PRCs (Honma et al., 2003), fast
44 re-entrainment after jet-lag (Yamazaki et al., 2000), and seasonal variability (Daan and Aschoff, 1975).

1.3 Empirical data as model constraints

46 In order to optimize phenomenological models, reasonable constraints based on experimental
47 observations have to be formulated. In mammals, the strong coupling of SCN neurons constitutes
48 a strong oscillator (Abraham et al., 2010; Granada et al., 2013) with quite small PRCs (Comas et al.,
49 2006). Even bright light pulses of 6.7h duration can shift the clock by just a few hours (Khalsa et al.,
50 2003). Consequently, we constrain our models to have small PRCs with just 1h advance and 1h delay.
51 Interestingly, despite the robustness of the SCN rhythms, a surprisingly fast recovery from jet-lag is
52 observed (Reddy et al., 2002; Vansteensel et al., 2003). Along the lines of a previous optimization study
53 (Locke et al., 2008), we request that our models reduce the jet-lag to 50% within 2 days. The third
54 constraint refers to the well-known seasonal variability of circadian clocks (Pittendrigh and Daan, 1976b;
55 Rémi et al., 2010). It has been reported that phase markers can lock to dusk or dawn for varying day-
56 length. This implies that the associated phases change by 4h, if we switch from 16:8 LD conditions to
57 8:16 LD conditions. Thus, we test whether or not our optimized models allow such pronounced phase
58 differences between 16:8 and 8:16 LD cycles.

2 METHODS

2.1 Optimization of amplitude-phase model

60 As a model of an autonomous circadian oscillator, we consider the following amplitude-phase model
61 (Abraham et al., 2010):

$$\frac{dr}{dt} = \lambda r(A - r), \qquad (1)$$

$$\frac{d\varphi}{dt} = \omega. \qquad (2)$$

62 The system is described in polar coordinates of radius r and angle φ, having a limit cycle with amplitude
63 A and angular frequency ω. Any perturbation away from the limit cycle will relax back with a relaxation
64 rate λ. This oscillator model can be represented in Cartesian (x, y)–coordinates as

$$\frac{dx}{dt} = -\lambda x(r - A) - \omega y + Z(t), \tag{3}$$

$$\frac{dy}{dt} = -\lambda y(r - A) + \omega x, \tag{4}$$

65 where $r = \sqrt{x^2 + y^2}$. The oscillator receives a *Zeitgeber* signal

$$Z(t) = \begin{cases} 1 & \text{if } t \mod T < \varkappa T \\ 0 & \text{otherwise},\end{cases} \tag{5}$$

66 where T represents the period of the *Zeitgeber* signal and $\varkappa$ determines the photoperiod (*i.e.*, fraction of
67 time during T hours when the lights are on). The amplitude–phase model provides one of the simplest
68 mathematical frameworks to study limit cycle oscillations, which have been discussed in the context of
69 circadian rhythms (Wever, 1962; Winfree, 1980; Kronauer et al., 1982).

70 The amplitude–phase model (1),(2) has three unknown parameters $\{A, \omega, \lambda\}$. These parameters were
71 optimized to satisfy the model constraints as described in 1.3. The parameter optimization is based on
72 minimization of a cost function. The cost function takes a set of parameters as arguments, evaluates the
73 model using those parameters, and then returns a "score" indicating goodness of fit. Scores may only be
74 positive, where the closer a fit gets to the score of zero, the better the fit becomes. The cost function is
75 defined as

$$E(A, \omega, \lambda) = \frac{(T_e - 48h)^2}{(24h)^2} + \frac{(\Delta\varphi_{max} - 1h)^2}{(1h)^2} + \frac{(\Delta\psi - 6h)^2}{(24h)^2}, \tag{6}$$

76 where T_e, $\Delta\varphi_{max}$, $\Delta\psi$ represent half-time to re-entrainment, maximum phase-shift, and seasonal phase
77 variability, respectively. The denominators can be regarded as tolerated ranges. If the values of T_e, $\Delta\varphi_{max}$,
78 and $\Delta\psi$ deviate 24h, 1h and $24h$ from their target values, a score of three results. All parameter sets
79 discussed in this paper had optimized scores below 0.1, i.e., the constrains are well satisfied. Each quantity
80 is defined and calculated as follows.

81 When the circadian oscillator is entrained to the *Zeitgeber* signal, their phase difference $\psi = \Psi - \varphi$
82 ($\Psi = 2\pi t/T$: phase of the *Zeitgeber*) converges to a stable phase ψ_e, that is called "phase of entrainment."
83 The half-time to re-entrainment T_e denotes the amount of time required for the oscillator to recover from
84 a jet-lag. As the *Zeitgeber* phase is advanced by $\Delta\Psi$, the phase difference becomes $\psi = \psi_e + \Delta\Psi$. T_e
85 quantifies how long it takes until the advanced phase is reduced to less than half of the original jet-lag
86 (*i.e.*, $|\psi - \psi_e| < 0.5\Delta\Psi$). In our computation, this quantity was averaged over 24 different times during
87 the day, at which 6h-advanced jet-lag was applied. Next, the seasonal phase variability, which quantifies
88 variability of the phase of entrainment over photoperiod from long day (16:8 LD) to short day (8:16 LD),
89 is computed as $\Delta\psi = \max_{\varkappa \in [1/3, 2/3]} \psi_e - \min_{\varkappa \in [1/3, 2/3]} \psi_e$. Finally, the maximum phase-shift is given
90 by $\Delta\varphi_{max} = \max_\varphi |PRC(\varphi)|$, where $PRC(\varphi)$ represents phase response curve of the free-running
91 oscillator, to which 6h light pulse is injected at its phase of φ.

92   To find optimal parameter values, the cost function was minimized by a particle swarm optimization
93   algorithm (Eberhart and Kennedy, 1995; Trelea, 2003). Search ranges of the parameter values were set to
94   $A \in [0, 5]$, $\omega \in [2\pi/30, 2\pi/18]$, $\lambda \in [0, 0.5]$. Altogether 300 sets of parameter values were obtained. From the
95   estimated parameters, the intrinsic period was obtained as $\tau = 2\pi/\omega$.

2.2   Simulations of jet-lag, phase response, and seasonality

97   Figure 1 illustrates our modeling approach. In Fig. 1a, the amplitude-phase equations (1) and (2) are
98   visualized in the phase plane together with the driving *Zeitgeber* switching between 0 (dark) and 1 (light)
99   for varying photoperiods. Two values of the amplitude relaxation rate λ illustrate how λ affects the decay
100 of perturbations. Starting from an initial condition, small relaxation rate gives rise to a long transient until
101 its convergence to limit cycle, while large relaxation rate exhibits only a short transient. Figure 1b shows
102 the oscillations in a 3-dimensional phase space. Two coordinates (x and y) span the phase plane of the
103 endogenous oscillator. The vertical axis represents the phase of the *Zeitgeber*. The red line marks the
104 periodically forced limit cycle. The jump from 24 h to 0 h reflects simply the periodic nature of our daily
105 time.

106   Interestingly, the relaxation after jet-lag (see also the more common presentations in Fig. 2) can be
107 visualized as a transient convergence to the red limit cycle via the black line after a 6h phase change due
108 to jet-lag (blue arrow). Such a relaxation might be accompanied by amplitude changes (not apparent) and
109 by steady phase shifts from day to day (note that the jump from 24 h to 0 h is shifted day by day). After a
110 few days, the red line is approached implying a vanishing jet-lag.

3   RESULTS

3.1   Models reproduce small PRC, short jet-lag, and seasonality

112   We performed 200 successful parameter optimizations leading to an ensemble of parameter sets. We
113 discuss in this section the parameters with a PRC of 1h delay and advance. In Figs. S1 & S2, we also
114 present a parameter set obtained with a modified optimization: in that case, we requested a PRC with 2h
115 delay and advance.

116   Figure 2 shows results for a representative model obtained via optimization. The PRC in Fig. 2a is
117 almost sinusoidal with maximal delays and advances of 1h as requested by optimization. Simulations
118 with different photoperiods are shown in Fig. 2b. It is evident that there are major phase shifts due to
119 varying photoperiods. The jet-lag visualized in Fig. 2c is surprisingly short for such a relatively small
120 PRC. Fig. 2d illustrates the re-entrainment after a jet-lag applied on day 10. Note, that no pronounced
121 amplitude changes were observed.

122   It is remarkable that such simple models with just three free parameters can reproduce phenotypic
123 features successfully. In particular, short jet-lag durations for quite small PRCs are surprising. In the
124 following we exploit the ensembles of parameter sets to understand the underlying principles.

3.2   Optimization produced highly clustered parameter sets

126   In this section, we focus on the 200 parameter sets with the ±1h PRCs exemplified in Fig. 2 (see Figs. S1
127 for ±2h PRCs).

128   The possible search ranges for our parameters were quite large (periods between 18 and 30h, amplitudes
129 between 0 and 5, and amplitude relaxation rates between 0 and $0.5h^{-1}$). The histograms from the

130 optimized parameter sets demonstrate that the search lead to quite specific values: amplitudes of about
131 2.1 ± 0.04, periods around 23.3 ± 0.1 h, and large relaxation rates of $0.4\pm0.1\,h^{-1}$.

132 The optimized amplitude can be easily understood from the constraint via PRCs: for a given pulse
133 strength the PRC shrinks monotonically with increasing amplitude (Pittendrigh, 1981; Vitaterna et al.,
134 2006). Consequently, the amplitude of about 2.1 implies a ±1h PRC. Indeed, our optimizations with a
135 ±2h PRC lead to smaller amplitudes around 1.2.

136 Amplitude relaxation rates range between 0.1 and $0.5\mathrm{h}^{-1}$. A value of $0.1\mathrm{h}^{-1}$ corresponds to a half-
137 life of the amplitude perturbations of about 7h, while a value of $0.5\mathrm{h}^{-1}$ corresponds to a half-life
138 of the amplitude perturbations of about 1.4h. Thus all values in the histogram imply relatively fast
139 amplitude relaxation. In Abraham et al. (2010), we termed limit cycles with fast amplitude relaxation
140 "rigid oscillators." Interestingly, Comas et al. (2007) found that light pulses separated by 10h shift phases
141 almost independently. This observation is consistent with fast amplitude relaxation rates. Jet-lag is a
142 specific type of a transient (compare Fig. 1b). Thus it seems reasonable that fast amplitude relaxation
143 helps to achieve short transients after a jet-lag.

144 The most surprising result of our optimization is the narrow range of intrinsic periods of about 23.3h. We
145 provide in the discussion arguments that specific periods allow appropriate seasonal flexibility (compare
146 Fig. 4). In short, at specific parts of *Arnold* onions (i.e. the entrainment regions in the $\varkappa - T$ parameter
147 plane), the required 4h phase differences are found giving a reasonable phase shifts between 16:8 LD and
148 8:16 LD.

149 Figure 3d illustrates that the optimized parameter values are not independent. For example, shorter
150 periods are associated with larger amplitude. A possible explanation is that short periods imply larger
151 effective pulse strength (a 6h pulse is than relatively long) leading to larger amplitude in order to have the
152 requested PRC amplitude.

153 In order to evaluate the robustness of our optimization approach, we generated also 100 parameter sets
154 with PRCs with about a 2h advance and delay. In these cases we found intrinsic periods of 24.6 ± 0.1 h and
155 amplitudes 1.15 ± 0.1. The relaxation rates and amplitude-period correlations were similar to the results
156 with PRCs of about 1h advance and delay, compare Fig. 3 and Fig. S1.

3.3   Arnold onions provide insights on the optimized parameters

158 To systematically investigate the impact of photoperiod ($\varkappa$) and Zeitgeber period (T) on entrainment
159 properties, we analyze in Figure 4 two *Arnold* onions for representative parameter sets with a short period
160 and a ±1 h PRC as well as a large period and a ±2 h PRC. Interestingly, the *Arnold* onions are tilted, *i.e.*
161 the DD periods at photoperiod $\varkappa = 0$ are smaller than the LL periods at photoperiod $\varkappa = 1$ as predicted
162 by *Aschoff's rule* for nocturnal animals (Aschoff, 1960). The largest entrainment range is found around
163 a photoperiod of 0.5 as predicted by Wever (1964). As expected, a larger PRC implies a wider range of
164 entrainment, compare sizes of the Arnold onion in Fig. 4 (a) and (b).

165 The phase of entrainment is color-coded in Fig. 4. It is evident that the phases vary strongly with
166 the external period T. There are theoretical predictions that phases change by about 12h (Wever, 1964;
167 Granada et al., 2013; Bordyugov et al., 2015) in the horizontal direction. Interestingly, the variation of
168 photoperiods in the vertical direction implies also very pronounced variations of the entrainment phase.
169 Consequently, we could find many parameter sets with about 4h phase shift between photoperiods of
170 $\varkappa = 1/3$ (8:16 LD) and of $\varkappa = 2/3$ (16:8 LD).

4 DISCUSSION

4.1 Optimized models reproduce phenotypic features

The circadian clock of vertebrates is characterized by a relatively small type 1 PRC, by a narrow entrainment range, by fast recovery from jet-lag, and by pronounced seasonal flexibility. We addressed the question whether or not these phenotypic features can be reproduced by simple amplitude-phase models with just 3 free parameters: period, amplitude, and relaxation time. To our surprise, we found many parameter sets via global optimization that reproduce the phenotypic features.

The availability of many parameter sets derived from random optimization allows extraction of essential properties of successful models. It turned out that the amplitude A is adjusted to reproduce small PRCs for a given *Zeitgeber* strength Z. According to limit cycle theory (Pavlidis, 1969; Peterson, 1980), the strength of a perturbation is governed by the ratio Z/A of *Zeitgeber* strength to amplitude. This implies that large limit cycles exhibit small PRCs for a fixed *Zeitgeber* strength (Vitaterna et al., 2006).

In all suitable models, we found relatively fast amplitude relaxation rates with half-lives of perturbations below 5h. This "rigidity" of limit cycles (Abraham et al., 2010) can support fast relaxation to the new phase after jet-lag (compare Fig. 1b). Interestingly, Comas et al. (2007) found that light pulses separated by 10h act almost independently. This observation is consistent with fast relaxation rates after light pulses.

In order to reproduce seasonality we optimized our model under the constraint that 16:8 and 8:16 LD cycles have entrainment phases that are about 4h apart. This implies that the phase could follow dusk or dawn (Daan and Aschoff, 1975). In other words, we requested that the entrainment phase depends strongly on the photoperiod. As illustrated in Fig. 4, such a strong dependency is indeed reproduced by our simple amplitude-phase models. Our optimization procedure selected specific periods that lead to a 4h phase variation between photoperiods $\varkappa = 1/3$ and $\varkappa = 2/3$. Note, that other periods can give large phase differences as well (compare the large vertical phase variations in Fig. 4).

4.2 Relevance of phenomenological amplitude-phase models

Simplistic models as studied in this paper are quite generally applicable. In principle, they could be used to describe single cells, tissue clocks, and organismic data. For single cells, damped stochastic oscillators can represent the observations also surprisingly well (Westermark et al., 2009). Such models have vanishingly small amplitudes, smaller relaxation rates, and are driven by stochastic terms. Otherwise their complexity is comparable to our models discussed above.

Complex models with multiple gene-regulatory feedback loops (Mirsky et al., 2009; Pokhilko et al., 2010; Relógio et al., 2011; Woller et al., 2016) could be reduced to amplitude-phase models simply by extracting periods, amplitudes, and relaxation rates from simulations. However, in such cases the amplitudes are not uniquely defined, since there are many dynamic variables.

4.3 How to define circadian amplitudes?

This difficulty to define amplitudes points to a general problem in chronobiology. Most studies focus on periods and entrainment phases. Limit cycle theory emphasizes that amplitudes are essential to understand PRCs and entrainment. It is, however, not evident which amplitudes properly represent the limit cycle oscillator. Some studies consider gene expression levels (Lakin-Thomas et al., 1991; Wang et al., 2019) or reporter amplitudes (Leise et al., 2012), and other studies quantify activity rhythms (Bode et al., 2011; Erzberger et al., 2013). Since the ratio of *Zeitgeber* strength to amplitude Z/A governs PRCs and

210 entrainment phases, we suggest that amplitudes could be quantified indirectly: the stronger the response
211 to physiological perturbations, the smaller the amplitude. This approach leads to the concept of strong and
212 weak oscillators (Abraham et al., 2010; Granada et al., 2013). Strong oscillators are robust and have small
213 PRCs and entrainment ranges but large phase variability (Granada et al., 2013). In this sense, wild-type
214 vertebrate clocks represent strong oscillators in contrast to single cell organisms or plants. Indeed, the
215 review of Aschoff and Pohl (1978) demonstrates impressively these properties.

216 Interestingly, a reduction in relative amplitudes (i.e., amplitudes as a fraction of the mesor) can reduce
217 jet-lag drastically, since resetting signals are much more efficient (Yamaguchi et al., 2013; An et al., 2013;
218 Jagannath et al., 2013).

4.4   Arnold onions quantify entrainment

220 As shown in Fig. 4, *Arnold* onions represent in a compact manner entrainment ranges and phases of
221 entrainment. Astonishingly, even quite basic models lead to really complex variations of entrainment
222 phases. As expected, the period mismatch $T-\tau$ has a rather strong effect on the entrainment
223 phase. This reflects the well-known feature that short intrinsic periods τ have earlier entrainment
224 phases ("chronotypes") (Pittendrigh and Daan, 1976a; Merrow et al., 1999; Duffy et al., 2001). These
225 associations are reflected in the horizontal phase variations in the *Arnold* onion. Interestingly, the vertical
226 phase variability is also quite large. This observation demonstrates that also the effective *Zeitgeber*
227 strength Z/A and the photoperiod affect the phase of entrainment strongly. Consequently, the expected
228 correlations between periods and entrainment phase could be masked by varying amplitudes, *Zeitgeber*
229 strength, and photoperiods. In other words, chronotypes are governed by periods only if relative *Zeitgeber*
230 strength and photoperiod are kept constant.

231 The complexity of entrainment phase regulation indicates that generic properties of coupled oscillators
232 can provide useful insight in chronobiology. In particular, basic amplitude-phase models can help to
233 understand the control of jet-lag and seasonality.

CONFLICT OF INTEREST STATEMENT

234 The authors declare that the research was conducted in the absence of any commercial or financial
235 relationships that could be construed as a potential conflict of interest.

AUTHOR CONTRIBUTIONS

236 H. H. designed the study. I. T. T. performed the model simulations. I. T. T., B. A., C. S., and H. H.
237 discussed the results. H. H. wrote the main text. I. T. T., B. A., and C. S. revised the text.

FUNDING

ACKNOWLEDGMENTS

REFERENCES

243 Abraham, U., Granada, A. E., Westermark, P. O., Heine, M., Kramer, A., and Herzel, H. (2010). Coupling
244   governs entrainment range of circadian clocks. *Molecular Systems Biology* 6, 438. doi:10.1038/msb.
245   2010.92

246 An, S., Harang, R., Meeker, K., Granados-Fuentes, D., Tsai, C. A., Mazuski, C., et al. (2013). A
247   neuropeptide speeds circadian entrainment by reducing intercellular synchrony. *Proceedings of the*
248   *National Academy of Sciences* 110, E4355–E4361

249 Aschoff, J. (1960). Exogenous and endogenous components in circadian rhythms. In *Cold Spring Harbor*
250   *symposia on quantitative biology* (Cold Spring Harbor Laboratory Press), vol. 25, 11–28

251 Aschoff, J. and Pohl, H. (1978). Phase relations between a circadian rhythm and its zeitgeber within the
252   range of entrainment. *Naturwissenschaften* 65, 80–84

253 Becker-Weimann, S., Wolf, J., Herzel, H., and Kramer, A. (2004). Modeling feedback loops of the
254   mammalian circadian oscillator. *Biophysical Journal* 87, 3023–3034

255 Bode, B., Shahmoradi, A., Rossner, M. J., and Oster, H. (2011). Genetic interaction of per1 and dec1/2
256   in the regulation of circadian locomotor activity. *Journal of Biological Rhythms* 26, 530–540

257 Bordyugov, G., Abraham, U., Granada, A., Rose, P., Imkeller, K., Kramer, A., et al. (2015). Tuning the
258   phase of circadian entrainment. *Journal of The Royal Society Interface* 12. doi:10.1098/rsif.2015.0282

259 Comas, M., Beersma, D., Spoelstra, K., and Daan, S. (2006). Phase and period responses of the circadian
260   system of mice (mus musculus) to light stimuli of different duration. *Journal of Biological Rhythms*
261   21, 362–372

262 Comas, M., Beersma, D., Spoelstra, K., and Daan, S. (2007). Circadian response reduction in light and
263   response restoration in darkness: a! Hskeleton ! 1light pulse PRC study in mice (mus musculus). *Journal*
264   *of Biological Rhythms* 22, 432–444

265 Daan, S. and Aschoff, J. (1975). Circadian rhythms of locomotor activity in captive birds and mammals:
266   their variations with season and latitude. *Oecologia* 18, 269–316

267 Daan, S. and Berde, C. (1978). Two coupled oscillators: simulations of the circadian pacemaker in
268   mammalian activity rhythms. *Journal of Theoretical Biology* 70, 297–313

269 Dibner, C., Schibler, U., and Albrecht, U. (2010). The mammalian circadian timing system: organization
270   and coordination of central and peripheral clocks. *Annual Review of Physiology* 72, 517–549

271 Dodd, A. N., Salathia, N., Hall, A., Kévei, E., Tóth, R., Nagy, F., et al. (2005). Plant circadian clocks
272   increase photosynthesis, growth, survival, and competitive advantage. *Science* 309, 630–633

273 Duffing, G. (1918). *Erzwungene Schwingungen bei veränderlicher Eigenfrequenz und ihre technische*
274   *Bedeutung*. 41-42 (F. Vieweg & Sohn)

275 Duffy, J. F., Rimmer, D. W., and Czeisler, C. A. (2001). Association of intrinsic circadian period with
276   morningness–eveningness, usual wake time, and circadian phase. *Behavioral Neuroscience* 115, 895–
277   899

278 Eberhart, R. and Kennedy, J. (1995). Particle swarm optimization. In *Proceedings of the IEEE*
279   *international conference on neural networks* (Citeseer), vol. 4, 1942–1948

280 Erzberger, A., Hampp, G., Granada, A., Albrecht, U., and Herzel, H. (2013). Genetic redundancy
281   strengthens the circadian clock leading to a narrow entrainment range. *Journal of The Royal Society*
282   *Interface* 10, 20130221

283 Forger, D. B. and Peskin, C. S. (2003). A detailed predictive model of the mammalian circadian clock.
284   *Proceedings of the National Academy of Sciences* 100, 14806–14811

285 Granada, A. E., Bordyugov, G., Kramer, A., and Herzel, H. (2013). Human chronotypes from a theoretical
286   perspective. *PLoS One* 8, e59464

287 Granada, A. E., Hennig, R. M., Ronacher, B., Kramer, A., and Herzel, H. (2009). Phase response curves:
288   elucidating the dynamics of coupled oscillators. *Methods in Enzymology* 454, 1–27

289 Hardin, P. E., Hall, J. C., and Rosbash, M. (1990). Feedback of the drosophila period gene product on
290   circadian cycling of its messenger RNA levels. *Nature* 343, 536–540

291 Hastings, M. H., Maywood, E. S., and Brancaccio, M. (2018). Generation of circadian rhythms in the
292   suprachiasmatic nucleus. *Nature Reviews Neuroscience* 19, 453–469

293 Honma, K.-i., Hashimoto, S., Nakao, M., and Honma, S. (2003). Period and phase adjustments of human
294   circadian rhythms in the real world. *Journal of Biological Rhythms* 18, 261–270

295 Huygens, C. (1986). *Horologium oscillatorium ("The pendulum clock, or geometrical demonstrations*
296   *concerning the motion of pendula as applied to clocks" translated by Richard J. Blackwell)* (Iowa State
297   University Press, Ames, Iowa)

298 Jagannath, A., Butler, R., Godinho, S. I., Couch, Y., Brown, L. A., Vasudevan, S. R., et al. (2013). The
299   CRTC1-SIK1 pathway regulates entrainment of the circadian clock. *Cell* 154, 1100–1111

300 Johnson, C. H. (1992). Phase response curves: what can they tell us about circadian clocks. In *Circadian*
301   *clocks from cell to human* (Hokkaido University Press, Sapporo), 209–249

302 Khalsa, S. B. S., Jewett, M. E., Cajochen, C., and Czeisler, C. A. (2003). A phase response curve to single
303   bright light pulses in human subjects. *The Journal of Physiology* 549, 945–952

304 Klotter, K. (1960). Theoretical analysis of some biological models. In *Cold Spring Harbor symposia on*
305   *quantitative biology* (Cold Spring Harbor Laboratory Press), vol. 25, 189–196

306 Kronauer, R. E., Czeisler, C. A., Pilato, S. F., Moore-Ede, M. C., and Weitzman, E. D. (1982).
307   Mathematical model of the human circadian system with two interacting oscillators. *American Journal*
308   *of Physiology-Regulatory, Integrative and Comparative Physiology* 242, R3–R17

309 Kuramoto, Y. (2012). *Chemical oscillations, waves, and turbulence*, vol. 19 (Springer Science & Business
310   Media)

311 Lakin-Thomas, P. L., Brody, S., and Coté, G. G. (1991). Amplitude model for the effects of mutations and
312   temperature on period and phase resetting of the neurospora circadian oscillator. *Journal of Biological*
313   *Rhythms* 6, 281–297

314 Leise, T. L., Wang, C. W., Gitis, P. J., and Welsh, D. K. (2012). Persistent cell-autonomous circadian
315   oscillations in fibroblasts revealed by six-week single-cell imaging of per2:: Luc bioluminescence.
316   *PloS One* 7, e33334

Leloup, J.-C. and Goldbeter, A. (2003). Toward a detailed computational model for the mammalian circadian clock. *Proceedings of the National Academy of Sciences* 100, 7051–7056

Locke, J. C., Westermark, P. O., Kramer, A., and Herzel, H. (2008). Global parameter search reveals design principles of the mammalian circadian clock. *BMC Systems Biology* 2, 22

Merrow, M., Brunner, M., and Roenneberg, T. (1999). Assignment of circadian function for the neurospora clock gene frequency. *Nature* 399, 584–586

Mirsky, H. P., Liu, A. C., Welsh, D. K., Kay, S. A., and Doyle, F. J. (2009). A model of the cell-autonomous mammalian circadian clock. *Proceedings of the National Academy of Sciences* 106, 11107–11112

Ouyang, Y., Andersson, C. R., Kondo, T., Golden, S. S., and Johnson, C. H. (1998). Resonating circadian clocks enhance fitness in cyanobacteria. *Proceedings of the National Academy of Sciences* 95, 8660–8664

Pavlidis, T. (1969). Populations of interacting oscillators and circadian rhythms. *Journal of Theoretical Biology* 22, 418–436

Pavlidis, T. (1973). The free-run period of circadian rhythms and phase response curves. *The American Naturalist* 107, 524–530

Peterson, E. L. (1980). A limit cycle interpretation of a mosquito circadian oscillator. *Journal of Theoretical Biology* 84, 281–310

Pikovsky, A., Rosenblum, M., and Kurths, J. (2003). *Synchronization: a universal concept in nonlinear sciences*, vol. 12 (Cambridge University Press)

Pittendrigh, C. S. (1981). Circadian systems: entrainment. In *Biological Rhythms* (Springer). 95–124

Pittendrigh, C. S. and Daan, S. (1976a). A functional analysis of circadian pacemakers in nocturnal rodents iv. entrainment: Pacemaker as clock. *Journal of Comparative Physiology* 106, 291–331

Pittendrigh, C. S. and Daan, S. (1976b). A functional analysis of circadian pacemakers in nocturnal rodents v. pacemaker structure: A clock for all seasons. *Journal of Comparative Physiology* 106, 333–355

Pokhilko, A., Hodge, S. K., Stratford, K., Knox, K., Edwards, K. D., Thomson, A. W., et al. (2010). Data assimilation constrains new connections and components in a complex, eukaryotic circadian clock model. *Molecular Systems Biology* 6, 416

Reddy, A., Field, M., Maywood, E., and Hastings, M. (2002). Differential resynchronisation of circadian clock gene expression within the suprachiasmatic nuclei of mice subjected to experimental jet lag. *Journal of Neuroscience* 22, 7326–7330

Relógio, A., Westermark, P. O., Wallach, T., Schellenberg, K., Kramer, A., and Herzel, H. (2011). Tuning the mammalian circadian clock: robust synergy of two loops. *PLoS Computational Biology* 7, e1002309

Rémi, J., Merrow, M., and Roenneberg, T. (2010). A circadian surface of entrainment: varying t, τ, and photoperiod in neurospora crassa. *Journal of Biological Rhythms* 25, 318–328

Schmal, C., Myung, J., Herzel, H., and Bordyugov, G. (2015). A theoretical study on seasonality. *Frontiers in Neurology* 6, 94

Strogatz, S. (2004). *Sync: The emerging science of spontaneous order* (Penguin UK)

Trelea, I. C. (2003). The particle swarm optimization algorithm: convergence analysis and parameter selection. *Information Processing Letters* 85, 317–325

Van der Pol, B. and Van der Mark, J. (1927). Frequency demultiplication. *Nature* 120, 363–364

Vansteensel, M. J., Yamazaki, S., Albus, H., Deboer, T., Block, G. D., and Meijer, J. H. (2003). Dissociation between circadian per1 and neuronal and behavioral rhythms following a shifted environmental cycle. *Current Biology* 13, 1538–1542

Vitaterna, M. H., Ko, C. H., Chang, A.-M., Buhr, E. D., Fruechte, E. M., Schook, A., et al. (2006). The mouse clock mutation reduces circadian pacemaker amplitude and enhances efficacy of resetting stimuli and phase–response curve amplitude. *Proceedings of the National Academy of Sciences* 103, 9327–9332

Wang, B., Kettenbach, A. N., Zhou, X., Loros, J. J., and Dunlap, J. C. (2019). The phospho-code determining circadian feedback loop closure and output in neurospora. *Molecular Cell* 74, 771–784

Westermark, P. O., Welsh, D. K., Okamura, H., and Herzel, H. (2009). Quantification of circadian rhythms in single cells. *PLoS Comput Biol* 5, e1000580. doi:10.1371/journal.pcbi.1000580

Wever, R. (1962). Zum Mechanismus der biologischen 24-Stunden-Periodik. *Kybernetik* 1, 139–154

Wever, R. (1964). Zum Mechanismus der biologischen 24-Stunden-Oeriodik: III. Mitteilung Anwendung der Modell-Gleichung. *Kybernetik* 2, 127–144

Winfree, A. T. (1980). *The geometry of biological time* (Springer-Verlag, New York, Heidelberg and Berlin)

Woller, A., Duez, H., Staels, B., and Lefranc, M. (2016). A mathematical model of the liver circadian clock linking feeding and fasting cycles to clock function. *Cell Reports* 17, 1087–1097

Yamaguchi, Y., Suzuki, T., Mizoro, Y., Kori, H., Okada, K., Chen, Y., et al. (2013). Mice genetically deficient in vasopressin v1a and v1b receptors are resistant to jet lag. *Science* 342, 85–90

Yamazaki, S., Numano, R., Abe, M., Hida, A., Takahashi, R.-i., Ueda, M., et al. (2000). Resetting central and peripheral circadian oscillators in transgenic rats. *Science* 288, 682–685
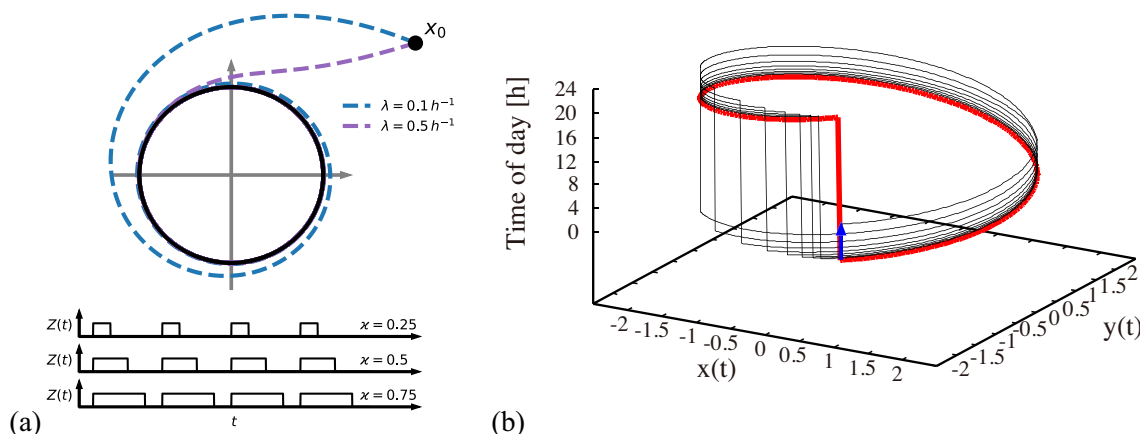
FIGURE CAPTIONS

Figure 1. Visualization of the amplitude-phase model. (a) Schematic illustration of the amplitude-phase oscillator model forced by a *Zeitgeber* (light) signal of different photoperiods $\varkappa$. Starting from the initial condition x_0, a small relaxation rate ($\lambda = 0.1\,\mathrm{h}^{-1}$) gives rise to long transient until its convergence back to the limit cycle, while transients for large relaxation rates ($\lambda = 0.5\,\mathrm{h}^{-1}$) are short. (b) The re-entrainment process of the oscillator after its phase is shifted by a 6h-advanced jet-lag. The red line represents the jet-lag shifted trajectory that the system converges to. The blue arrow indicates the 6h jet-lag.
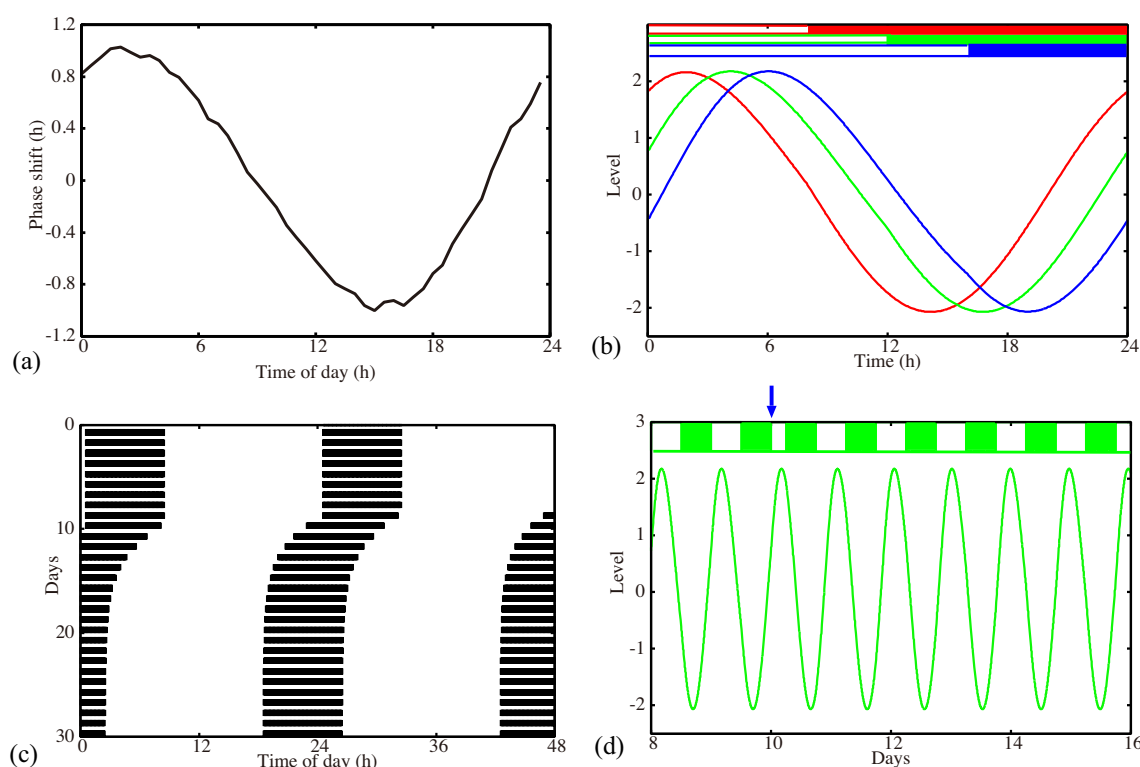

Figure 2. Properties of our amplitude-phase model for a representative optimized parameter set. (a) Phase response curve with respect to 6h light pulse. (b) Waveforms $x(t)$ of the oscillator entrained to *Zeitgeber* signal with 8:16 LD (red), 12:12 LD (green), and 16:8 LD (blue). (c) Actogram drawn for the oscillators, to which a 6h advancing jet-lag was induced on day 10. (d) Time-trace $x(t)$ of the oscillators, to which a 6h advancing jet-lag was induced on day 10. Model parameters: $\tau = 23.36$h, $A = 2.063$, $\lambda = 0.386$h^{-1} with $\omega = \frac{2\pi}{\tau}$.
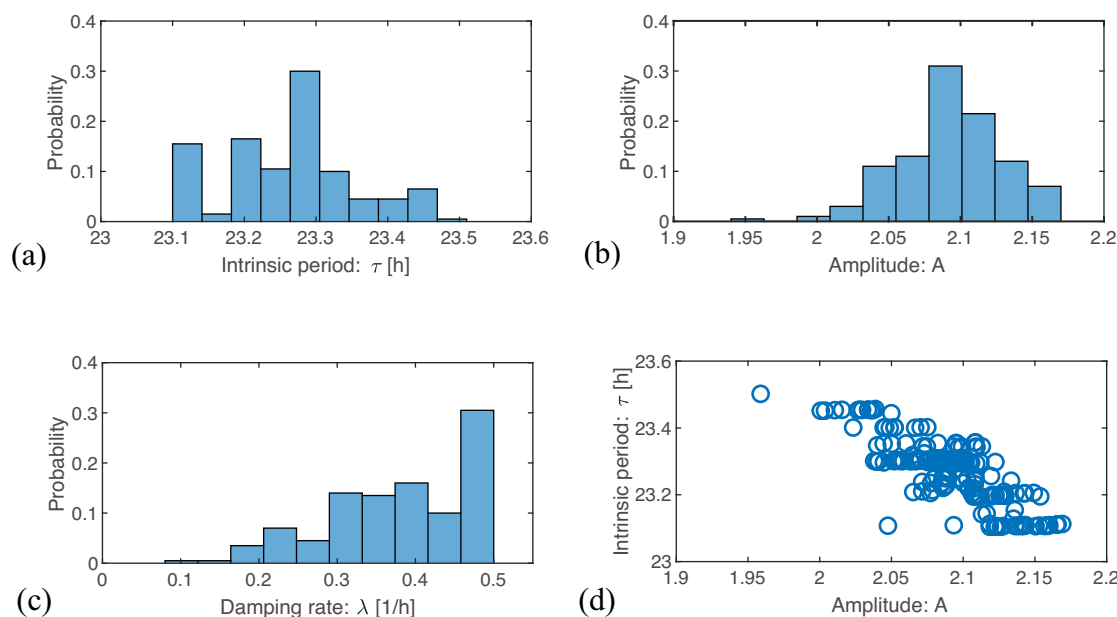
Figure 3. Parameter values in the optimized ensemble. (a-c) Distributions of the optimized parameter values for $\tau \ (= 2\pi/\omega)$, A, and λ, respectively. (d) Scatter plots of amplitude A against intrinsic period τ drawn for the 200 sets of optimized parameters.
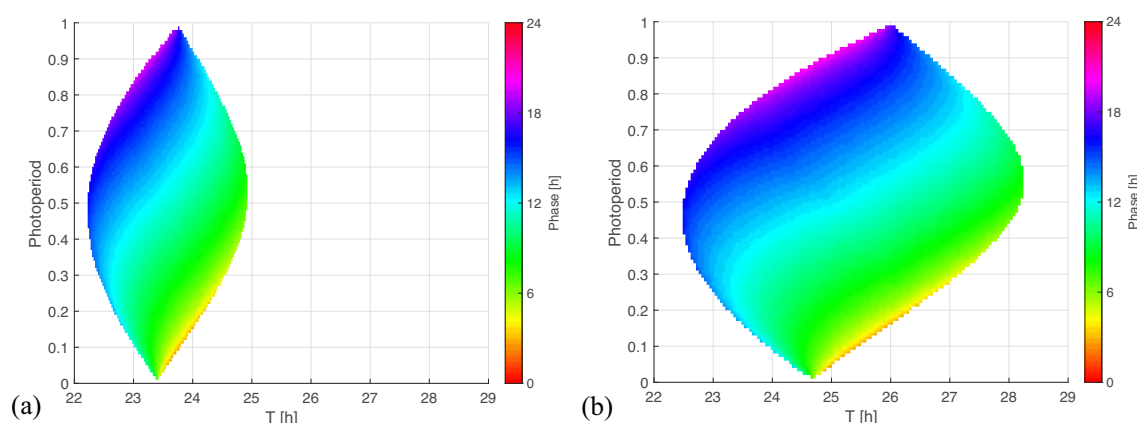

Figure 4. *Arnold* onions for the two PRC constraints. (a,b) 1:1 entrainment ranges in the $\varkappa$-T parameter plane (*Arnold* onions). Entrainment phases were determined by numerical simulations and have been color-coded within the region of entrainment. Panel (a) depicts an *Arnold* onion for an optimized parameter se with a $\pm$1h-PRC, a short-period $\tau = 23.36$h, $A = 2.063$, and $\lambda = 0.386$h^{-1}. Panel (b) shows an *Arnold* onion for an optimized parameter set with a $\pm$2h-PRC, a long-period $\tau = 24.64$h, $A = 1.144$, $\lambda = 0.50$h^{-1}.
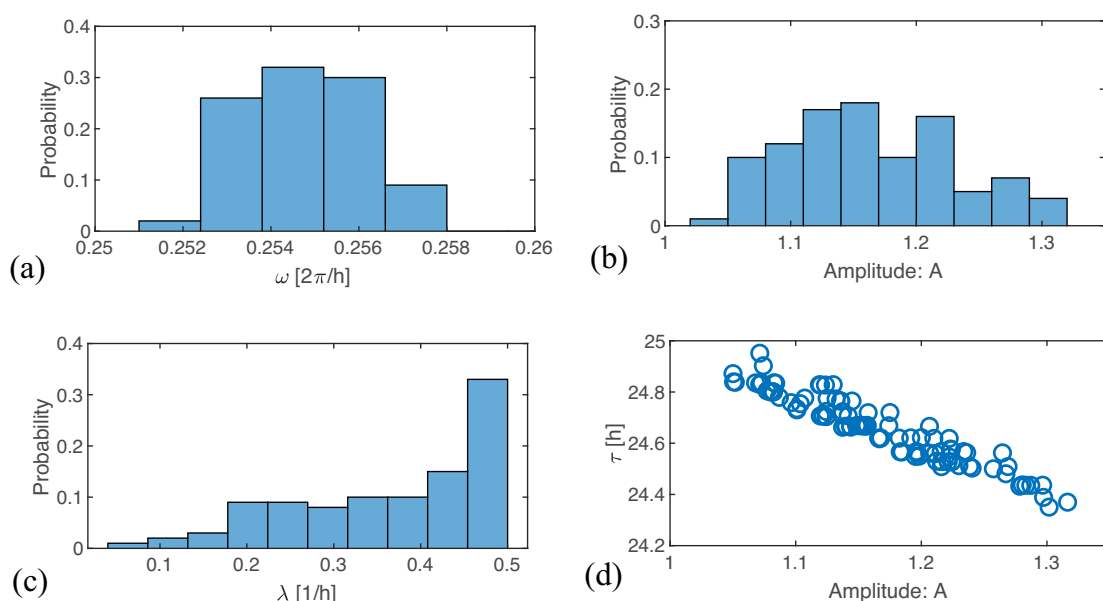
Figure S1. Results of parameter optimization based on cost function $E(A, \omega, \lambda) = \frac{(T_e - 48)^2}{(24)^2} + \frac{(\Delta\varphi_{max} - 2)^2}{(1)^2} + \frac{(\Delta\psi - 6)^2}{(24)^2}$, where ± 2h PRC was requested. (a-c) Distributions of the 100 optimized parameter sets for τ (24.6±0.16 h), A (1.2±0.07), λ (0.37±0.12), respectively. (d) Scatter plots of amplitude A against intrinsic period τ drawn for 100 sets of optimized parameters.
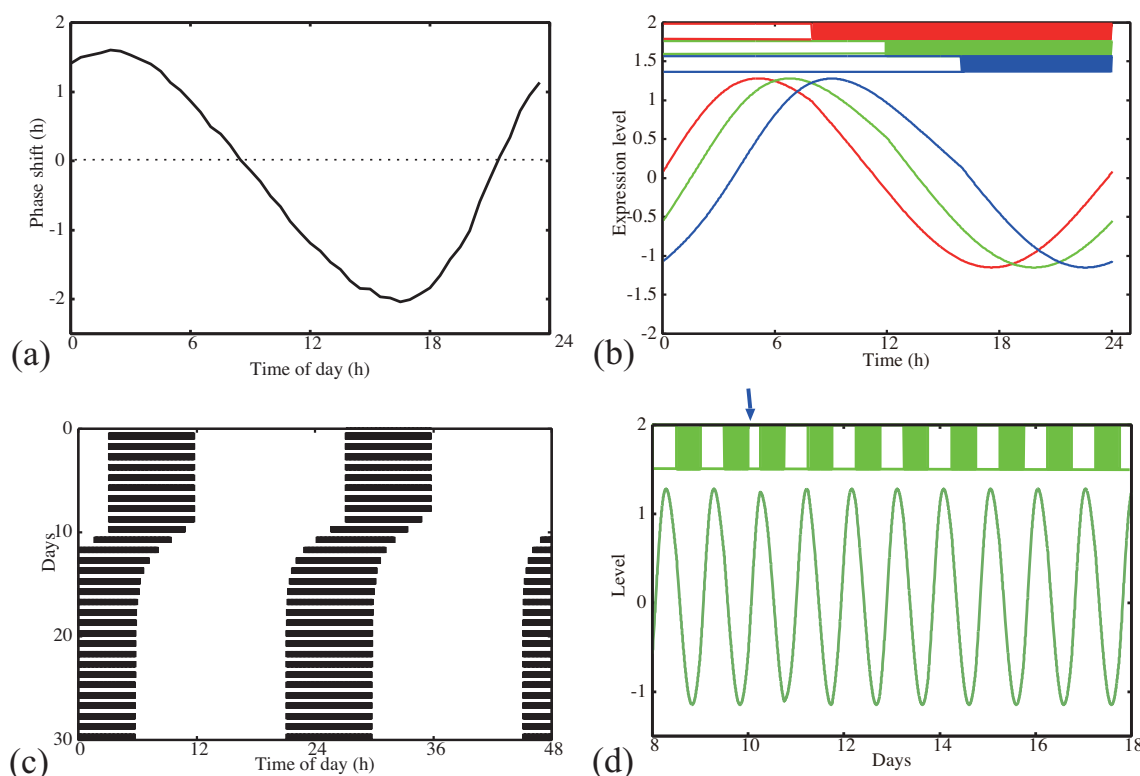
Figure S2. Simulation of the amplitude-phase oscillator model using one of the 100 parameter sets optimized for a ±2h PRC. (a) Phase response curve with respect to 6h light pulse. (b) Waveforms $x(t)$ of the oscillator entrained to *Zeitgeber* signal with 8:16 LD (red), 12:12 LD (green), and 16:8 LD (blue). (c) Actogram drawn for the oscillator, to which a 6h advancing jet-lag was induced on day 10. (d) Time-trace $x(t)$ of the oscillators, to which a 6h advancing jet-lag was induced on the 10th day. Parameter values: $\tau = 24.64$h, $A = 1.144$, $\lambda = 0.50$h^{-1}.